Cement and Concrete Composites 75 (2017) 10–21

Contents lists available at ScienceDirect

Cement and Concrete Composites

journal homepage: www.elsevier.com/locate/cemconcomp

Synthesis, characterisation and performance of piezo-resistive cementitious nanocomposites

Saptarshi Sasmal*, N. Ravivarman, B.S. Sindu

Structural Engineering Research Center (CSIR-SERC), CSIR, Taramani, Chennai, 600113, India

ARTICLE INFO

Article history:
Received 21 January 2016
Received in revised form
9 September 2016
Accepted 9 October 2016
Available online 11 October 2016

Keywords:
Multi walled carbon nanotubes (MWNTs)
Surfactant
Dispersion
Cyclic loading
Piezo-resistivity
Conductance
Nano-composite

ABSTRACT

Smart material reinforced non-destructive structural health monitoring technique has been evolving as the most predominated route for assessing the performance of the civil structures. In the present study, multiwalled nanotubes (MWNT) were suitably incorporated into the cement matrix, which act as actively embedded sensor for monitoring real-time flaws in structures. Initially, the stable homogenous MWNT dispersion was prepared by using ionic surfactant technique with high-intensity ultrasonic agitation process. Since, a suitable and adequate synthesis procedure to incorporate MWNT in cement matrix is essential, but complicated, the role of amplitude and frequency of sonication on dispersion of nanotubes was categorically evaluated. Further, this paper focuses to find out the effect of surfactant on MWNT dispersion by using the UV Visible spectroscopy and by evaluating the effective hydro-dynamic diameter. Based on micromechanics based analytical model, the influence of the interface layer thickness and geometrical configuration of nanotubes on the electrical conductivity of cement nano-composite are also analyzed. Further, the electrical conductivity of MWNT incorporated cement system, as developed in the present study, is measured using four probe method. Piezo-resistivity of the oven dried samples is measured to evaluate the change in potential drop under cyclic loading regime. It is found that the efficiency of the piezo-resistive strain sensors greatly depends on synthesis process and the circuit system. Appropriately proportioned and properly synthesized MWNTs incorporated in cement matrix were capable of providing consistent and steady response under the variable external stress. Thus, the material can be used as embedded sensor for health monitoring and identifying initiation of any damage in reinforced concrete structure.

1. Introduction

As the structures are getting older and deteriorated, awareness on the effects of extreme events in civil infrastructure is growing very fast. Research community needs advanced tools to monitor the health condition of the civil structures. Due to the inherent properties of reinforced concrete structures, damage progression inside the structure needs regular monitoring to avoid any catastrophic failure and loss of life and property. Generally, health monitoring of structures is carried out by affixing electric resistance strain gauges on the concrete surface using special type of conductive adhesive. These metal foil strain sensors have some limitations like low gauge factor, field effect, drift due to temperature sensitivity, long term change in foil conductivity and requirement of abundant amount of electric energy for operation. Most of the times, this technique of strain measurement (externally affixing) provides incorrect signals due to undesirable performance of the conductive adhesive and/or the malfunctioning of the electric resistance strain gauge. Hence, there is a need for an alternate and smarter solution to monitor the stress state of structures. Chen and Chung opened a door for the civil engineering community by successfully reinforcing short carbon fiber (0.2–0.4%) into cement matrix to yield smart concrete for non-destructive damage monitoring [1]. Later, the electrical conductivity of carbon fiber incorporated cement composite was used to develop embedded type sensor [2]. Since then, efforts are being made for engineering the cement composite with conductive particles and semi conductive fillers such as carbon coated nickel fiber, brass coated steel fiber, carbon black and various nano-phase materials.

Recent advancements in nanotechnology have given a pathway

* Corresponding author. Nano-Infra Engineering Group and Bridge Engineering Group, CSIR-Structural Engineering Research Center (CSIR-SERC), CSIR Complex, Taramani, Chennai, 600113, India.
E-mail addresses: saptarshi@serc.res.in, sasmalsap@gmail.com (S. Sasmal).

http://dx.doi.org/10.1016/j.cemconcomp.2016.10.008
0958-9465/

to develop new cement-based nano-composites which can be used as in-built sensors. Carbon nanotube (CNT) is an infinitesimal sized material which possesses superior morphology, structural stability, electrical conductivity [3] and electro-mechanical property [4]. The emerging field of carbon nano-engineering offers an approach to incorporate or embed CNT element in cementitious matrix by exploiting larger surface area and meso-pore reduction effect [5]. Even small amount of nano-filler (CNT), which has high aspect ratio, can be incorporated as second phase into an insulating matrix to achieve electrically conductive network without any adverse effect on mechanical property of the base composite [6]. Electrical properties, such as resistance and reactance, of these composites can vary with respect to externally applied stress [4]. This property indicates that an ordinary composite matrix can be transformed into a strain sensitive matrix i.e., the matrix with pressure sensitivity (piezo–resistivity sensor) through suitable nano-engineering. As a result, it will not only help in monitoring the overall structural health but will also help in determining the information about microstructural deformation of the matrix [7]. Thus, CNTs can be used as the next generation multi-functional conductive nanofillers to develop smart nano-composites.

The role of nano fiber dispersion is found to be one of the key factors to establish efficient electrical conductive network in cement matrix. Due to the intrinsic van der Waals interaction [estimated to be 500 eV/μm] [8], nano tubes tend to form tangles which provide major obstacle to transfer the extraordinary properties of CNT to the CNT reinforced composites. These effects can be eliminated by achieving uniform homogenous aqueous dispersion of CNT through chemical treatment (covalent functionalization) or dispersing agent (surfactant). Obviously, the covalent bond (CB) functionalization achieved by exploiting CB and amine acidic reactions prompt the functional group to form conjugated π-electron system. Thus, the distortion in the CNT structure takes place. It is reported that the increased affinity between matrix and nanotubes causes the reduction in the maximum conductivity of composite matrix. Alternatively, the typical non-covalent interaction (ionic–surfactant assisted process) with hydrophilic head and hydrophobic tail groups effectively exfoliate the CNT bundle into single tube which ensures the stable dispersion without any detrimental effect in the conduction properties of CNT [6 and 9].

Han et al. was the first one to investigate the effect of sodium dodecyl benzene sulfonate (SDBS) ionic surfactant to disperse carboxyl MWNTs for piezo-resistive response of cement based composite [10]. They were able to achieve excellent piezo-resistivity by adding just one tenth of nano fiber than that reported in previous study [11]. This is due to the presence of benzene ring in hydrophobic chain, so_3^{2-} head group and longer alkyl chain in the utilized ionic surfactant. Even though the method is beneficial for stable dispersion, due to air entrapment it brings some negative effect on mechanical properties of cementitious matrix [12]. Further, higher surfactant doping causes negative effect during cement hydration [13,14]. It is also reported that excess surfactant obstructs the direct electrical contact between the neighbouring CNTs and produces higher noise to signal ratio [13]. In order to increase the higher signal to noise ratio and to provide the stable charging-discharging effect of capacitance of MWNT/cementitious composite, low amplitude AC voltage instead of DC supply can be given [15]. Additionally, the noise that is captured along with the signal could be minimised by employing small quantity of CNT (1% CNT for 15% CNF) [16]. The stable sensitivity of the nano-composite is realized after 28 days of curing [17]. Also, the sensitivity of matrix is improved through alignment of CNTs in composite matrix. This produces higher gauge factor especially in cross-flow direction. Moreover, the random fiber orientation offers formation of electrically conductive network in composite matrix, but significantly reduce the matrix sensing capacity due to the reduction of tunnelling gap among CNTs [18,19]. Further, CNT reinforced composite matrix exhibits its sensitivity under compressive loading. Further, dynamic test also reveals that it can track the excitation frequency range from 0.25 to 15 Hz. At the same time, this frequency range lies in line with capacitor fabricated from a nano-composite mix [20]. The well dispersed and clustered nature of nanofiber in cement paste facilitates to produce C-S-H products over the surface of fillers during hydration period of cement composites. Therefore, the intrinsic properties of nanofiber successfully can be transferred to cement matrix [21,22]. Also, the straightness of the nanofiber results in greater flexure strength via anchoring mechanism [23]. Electro-mechanical properties of nano composites for dynamic sensing were discussed in Refs. [24,25].

From the exhaustive review of literature, it is found that many attempts have been made to incorporate the conductivity in cement matrix by using various types of fibers. The performance of CNT incorporated cement system for piezo-resistivity greatly depends on the quality of dispersion. The issues like the ability of various surfactants on MWNTs dispersion, dispersability and particle size distribution of CNTs as function of sonication time, effect of surfactant concentration to reinforce CNT in cement mortar and ultrasonic energy are discretely addressed by few researchers [26–29]. Procedure for preparation of CNT/concrete composite using ultrasonic process was demonstrated by Han et al. [30]. It is also reported that sonication energy causes the decrease in the aspect ratio of fiber which subsequently reduces the electrical conductivity. At the same time, self-sensing ability of cement based composites in large scale is reported to have limited success [31]. In view of this, it is to mention that the entire procedure, namely, sonification and/or centrifuge, dispersion, addition of CNT dispersed aqueous solution in cement matrix and development of the CNT incorporated cement system are extremely crucial and not straight forward. Nevertheless, though significantly important, there is no clear understanding on the relation among the electrical conductivity of CNT/CNF filled cementitious composite with the role of ultrasonic energy, hydrodynamic diameter of dispersed MWNTs, and surfactant concentration. Hence, it is required to carry out a thorough investigation to provide systematic procedure for the synthesis, development and performance evaluation of the nano engineered cement composite with strain sensing capabilities. Further, most of the reported studies chose the type of CNT/CNF in ad-hoc manner and no scientific approach is reported in selecting the physical parameters of the nanofibers. In this present work, the study is initially focused on the micromechanics based analytical investigations to identify the influence of geometry of CNT on the conductivity and to assess the effective electric percolation network in cement matrix. Further, this study illustrates the role and effect of ionic surfactant (SDBS) concentration and various parameters of ultrasonication on the CNT hydrodynamic diameter which helps in establishing the procedure for synthesis of the nano-composite. Then, the aspects such as spacing between embedded voltage and current terminals, correlation between matrix microstructure deformation and changes in composite conductance with the influence of varying input level under cyclic compressive loading regime, are discussed. Finally, the study demonstrates the development of the piezo-resistive cementitious nano-composite for strain sensing application.

2. Selection of nano fibers

To produce electrically conductive nano-composite, critical volume fraction of fiber is an essential parameter to create the conductive percolation threshold in composite matrix. Besides, the intrinsic physical characteristics such as aspect ratio and electrical

conductivity of fiber along its geometry are very important. To judiciously choose the appropriate fiber with effective reinforcing effect, a nano-scale RVE of CNT incorporated matrix from microscopic RVE, as shown in Fig. 1, is considered. It consists of a hollow nano-filler (CNT) and the continuum interface layer of thickness "t" around CNT. It is clear from the nano-scale RVE that the electrical conductivity of composite can be determined through three approaches, i) electrical conductivity of CNT, ii) conductivity of interface layer, and iii) electron hopping transport through interface. The entire mechanism with the coordinate system is schematically presented in Fig. 1.

Considering a uniform external electrical field E_0 applied in the plane of lamellae of composite matrix containing randomly distributed CNTs, the effective electrical conductivity along longitudinal direction in local coordinate system can be determined by using law of mixture. As a result, the effective longitudinal conductivity in the local coordinate system is estimated as [32],

$$\sigma^{L}_{local} = \frac{\sigma^{L}_{c} r_c^2 + \sigma_{int}(2r_c t + t^2)}{(r_c + t)^2} \tag{1}$$

where, σ^{L}_{c}, σ_{int} are the electrical conductivities of the CNT along the longitudinal direction and the interface, respectively. r_c is the radius of nano filler and t is the interface thickness around the nano filler.

Due to the variation in cylindrical surface area along the transverse direction, Maxwell's equation in the local polar coordinate can be employed to determine the transverse electrical conductivity of the composite. When a system is subjected to a uniform external electrical field (E_0) along the arbitrary radial direction, the system can be represented as

$$\nabla^2 \varphi = \frac{1}{r}\frac{\partial}{\partial r}\left(r\frac{\partial \varphi}{\partial r}\right) + \frac{1}{r^2}\frac{\partial^2 \varphi}{\partial \theta^2}, \tag{2}$$

where φ is the electrical potential in the (r, θ) coordinate system.

Finally, by applying the prescribed boundary condition, the effective electrical conductivity in longitudinal and transverse direction in the local coordinate system is obtained by Yan et al. [33] and is given below.

$$\sigma^{T} = \frac{\sigma_{int}}{L + 2t}\left[L\frac{2r_c^2\sigma_c^T + (\sigma_c^T + \sigma_{int})(t^2 + 2r_c t)}{2r_c^2\sigma_{int}^T + (\sigma_c^T + \sigma_{int})(t^2 + 2r_c t)} + 2t\right] \tag{3}$$

$$\sigma^{L} = \frac{(L + 2t)\sigma_{int}\left[r_c^2\sigma_c^L + \sigma_{int}(t^2 + 2r_c t)\right]}{2r_c^2\sigma_c^L t + 2\sigma_{int}(t^2 + 2r_c t)t + \sigma_{int}L(r_c + t)^2} \tag{4}$$

where, σ^T, σ^L & σ_c^T, σ_c^L denote the effective electrical conductivity of composite and CNT along transverse and longitudinal direction, respectively. r_c, t, & σ_{int} denote the fiber radius, thickness of interface layer and interface electrical conductivity. The local electrical conductivity of CNT is assumed to be $1 \times 10^3\ \Omega^{-1}\ m^{-1}$ along longitudinal direction and $1 \times 10^2\ \Omega^{-1}\ m^{-1}$ along transverse direction, as reported in Ref. [34].

Fig. 2 shows the effective electrical conductivity spectra of CNT incorporated composite verses electrical conductivity of interface layer where longitudinal and transverse conductivity of CNT, fiber radius, & thickness of interphase (interface) layer are the parameters. The envelops of longitudinal and transverse conductivity with the change in radius and longitudinal conductivity of CNT and thickness of interphase layer were plotted using Equations (3) and (4) and shown in Figs. 2 and 3. From Fig. 2(a), it is found that the longitudinal effective electrical conductivity of composite shows steadily increased response with change in longitudinal electrical conductivity of CNT. Therefore, the intrinsic electrical conductivity of CNT along the axial direction plays a major role to activate the composite matrix as electrically conductive along longitudinal direction. Similarly, it can be observed from Fig. 3(a) that with change in transverse electrical conductivity of CNT, there is a steady increase in transverse electrical conductivity of the matrix (before the saturation state). It is also interesting to note that the increase in composite conductivity with the improvement in longitudinal conductivity of CNT (at initial stage) is much higher than that observed from change in transverse conductivity. The influence of fiber radius, r_c on the longitudinal and transverse conductivity of matrix is also studied. It is to note that with the increase in the radius of CNT, composite conductivity reduces and the reduction is more prominent with higher interphase conductivity (Figs. 2(b) and 3(b)). However, the interphase thickness helps in improving the conductivity of the composite (Figs. 2c) and 3(c)).

The influence of fiber radius on the conductivity can be

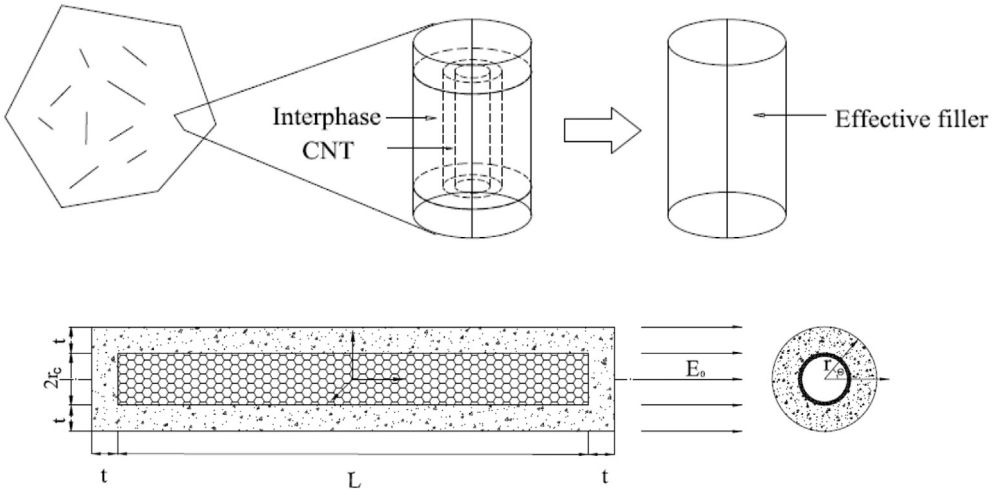

Fig. 1. Schematic view of CNT nano-composite consisting of randomly oriented CNTs.

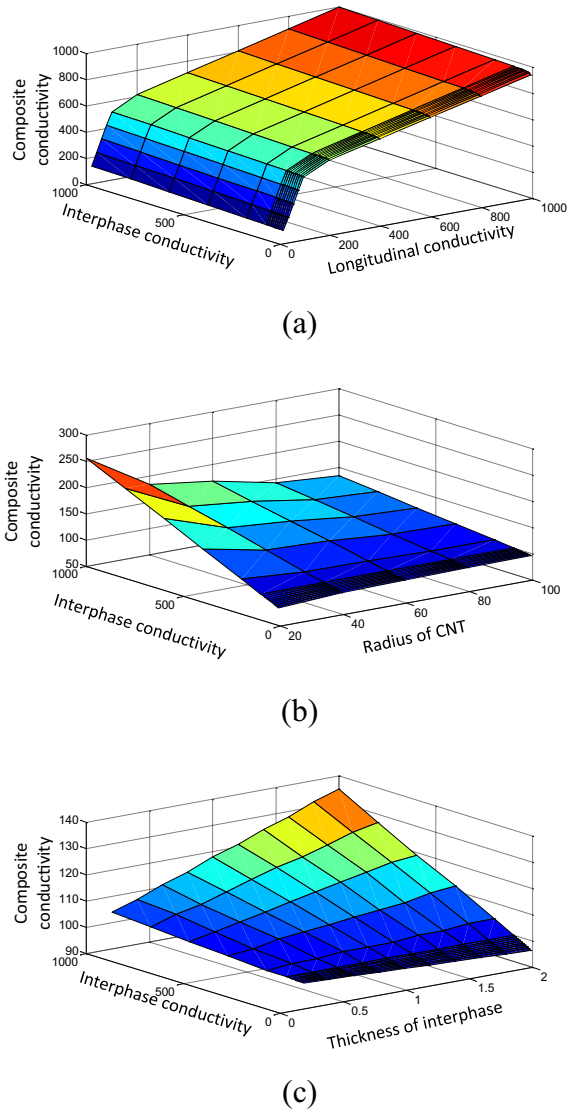

Fig. 2. Longitudinal electrical conductivity characteristic of CNT reinforced composite with respect to (a) different CNT longitudinal conductivity, (b) radius of CNT, (c) thickness of interphase layer "t" [Conductivity is denoted as $\Omega^{-1}m^{-1}$ and dimensions are in nm].

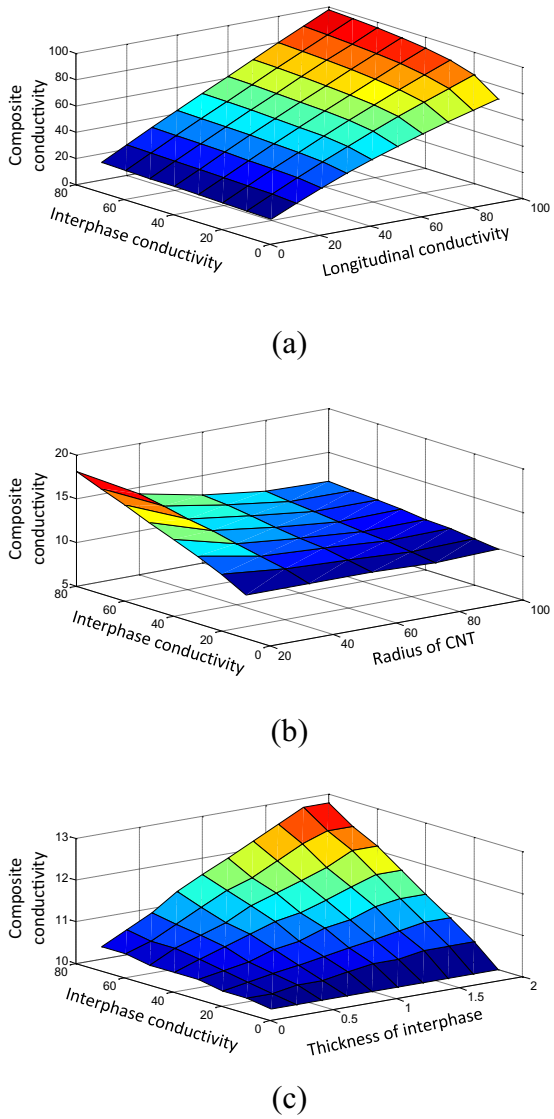

Fig. 3. Transverse electrical conductivity characteristic of CNT reinforced composite with respect to (a) different CNT longitudinal conductivity, (b) radius of CNT, (c) thickness of interphase layer "t" [Conductivity is denoted as $\Omega^{-1}m^{-1}$ and dimensions are in nm].

understood by assuming CNT as a hollow cylindrical tube. Considering a differential element which is made up of thin cylinder of inner radius, r, outer radius, $r + \partial r$ and length, l, resistance of system can be given by,

$$\partial R = \frac{\rho \partial l}{A} = \frac{\rho r \partial r}{2\pi r l} \tag{5}$$

where, $A = 2\pi r L$ is the area normal to the direction of current flow.

The total resistance of the system then becomes,

$$R = \int_{r}^{r+\partial r} \frac{\rho r \partial r}{2\pi r l} = \frac{\rho}{2\pi l} \ln\left[\frac{b}{a}\right] \tag{6}$$

By substituting the values of upper and lower limits, we can realize that the resistance of hollow cylindrical fiber is inversely proportional to fiber radius. If the values of a and b are same, the observed fiber conductivity will be maximum, i.e., $R = 0$.

The change in conductivity of matrix with the variation of the interface thickness, t is shown in Figs. 2(c) and 3(c). Both the plots indicate that the total conductivity of the matrix increases with increase in the thickness of interface layer which is around the CNT surface (i.e., the total matrix conductivity is the sum of fiber and interface conductivity). This holds true only when the interface layer has conductive property. Since, cementitious matrix possesses weak electrical conductivity, the whole matrix conductivity is almost independent of interface layer thickness, t. From the above observation, it has been identified that CNTs of smaller radius offers better conductivity. Hence, in this study, fiber of radius 50–80 nm, length of 15 μm and conductivity in the range of (1.34–1.19) $x10^1$ Ω^{-1} m^{-1} in transverse direction and (1.43–1.68) $x10^2$ $\Omega^{-1}m^{-1}$ in longitudinal direction is considered. To evaluate the influence of interface layer thickness on the longitudinal and transverse conductivity, the range of interface layer is chosen from the reported literature [35]. In the present study, the interface layer is considered to be conductive but not capacitive.

3. Materials and preparation

3.1. Materials

Cement mortar was prepared with ordinary Portland cement of Grade 53 (density-3150 kg/m^3) and fine aggregate (density-2600 kg/m^3) of size less than 2 mm. Water to cement ratio was kept as 0.35. MWNTs were purchased from Nanostructure and Amorphous Materials, Inc. Houston, Texas. The chemical composition and physical properties of the MWNTs is given in Table 1. It is to mention that MWNT with smaller diameter is commercially available at low cost. Sodium dodecyl benzene sulfonate (348.48 MW, 80% assay) was used as dispersing agent and tributyl phosphate was used as deformer.

3.2. Preparation of MWNT dispersion

MWNTs were added to the ionic surfactant at a concentration of 0.005 g/ml. The aqueous solution was stirred using magnetic stirrer for 10 min. Subsequently, the solution was subjected to ultrasonic agitation process at room temperature. During ultrasonication, duration, amplitude and frequency of sonication were varied to determine the optimum parameters. Further, the influence of the surfactant to nanotube ratio (S/C) on the dispersion was studied. The aqueous MWNT dispersion prepared by various methods is shown in Fig. 4. Fig. 4(a) and (b) depict the water dispersed sample (shows rapid sedimentation) and the surfactant dispersed sample, respectively. There is a reduction in the deposition of CNTs in this case due to steric repulsion. The other two samples shown in Fig. 4(c) and (d) are prepared through ultrasound agitation process which show improved dispersion.

4. Characterisation techniques

4.1. UV–visible spectrum

The stability of surfactant assisted aqueous MWNTs dispersion is characterized using UV–Vis spectroscopy (MODE–DRS, Carry 5000 UV-VIS NIR, Agilent Technologies) operated at 200–800 nm range. Fig. 5(a) and (b) show the absorbance spectra of aqueous solution with different surfactant to MWNT ratio (S/C of 0.4, 0.5, 0.6 and 0.7) subjected to sonication (50% amplitude & 50% cycle) and centrifugation (10 M, 3000 rpm) for a duration of 15 min and 30 min, respectively. Centrifugation was carried out after the sonication. The nomenclature of 'AS' is used for samples subjected to only sonication, and 'AC' is used for samples subjected to sonication followed by centrifugation (as given in Table 2). It can be observed from the figures that the spectra of all the samples showed rapid increase in absorbance upto 349 nm. This may be due to the π-π stacking interaction between benzene ring of ionic surfactant and graphite surface [36,37]. Then, there is a sudden drop in absorbance which is followed by monotonic decrease from 350 nm to 800 nm. This is primarily coupled with light scattering from carbon particles in the dispersion medium.

The absorbance of all the samples at 349 nm is presented in Table 3. Samples with S/C of 0.5 and 0.6 agitated for 15 min had similar absorbance even after being subjected to centrifugation. This shows that the solution is well dispersed. It is to be noted that sample with S/C of 0.4 showed 13% lesser absorbance when subjected to centrifugation. This means that the amount of surfactant used in this case was not sufficient to disperse all CNTs which caused agglomeration and settling down of CNTs. The sample with S/C of 0.7 also showed reduction in absorbance after centrifugation. In this case, the surfactant particles would have flocculated due to their higher concentration which further causes poor dispersion of CNTs [38]. However, all the samples agitated for 30 min showed similar absorbance even after being subjected to centrifugation. This shows that duration of sonication has a major role in proper

Table 1
Physical properties of MWNT and chemical composition of MWNT.

Appearance	Outer diameter	Inner diameter	Length	Purity
Black	50–180 nm	5–15 nm	50–80	>95%
Components	C	Cl	Fe	Ni	S
Contents (%)	97.37	0.20	0.55	1.86	0.02

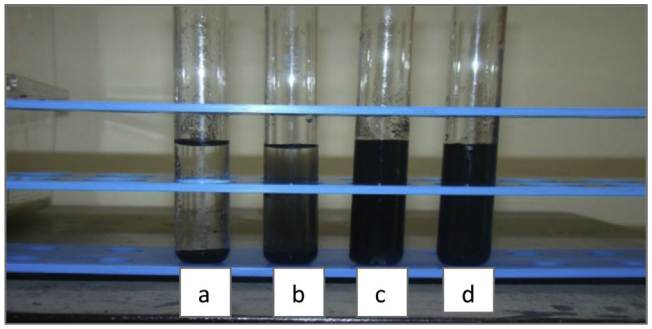

Fig. 4. Image of MWNT dispersed solution a) MWNT + Water b) MWNT + Water + SDBS c) MWNT + Water + SDBS + Sonication d)) MWNT + Water + SDBS + Sonication + centrifuge at 3000 rpm for 10 M.

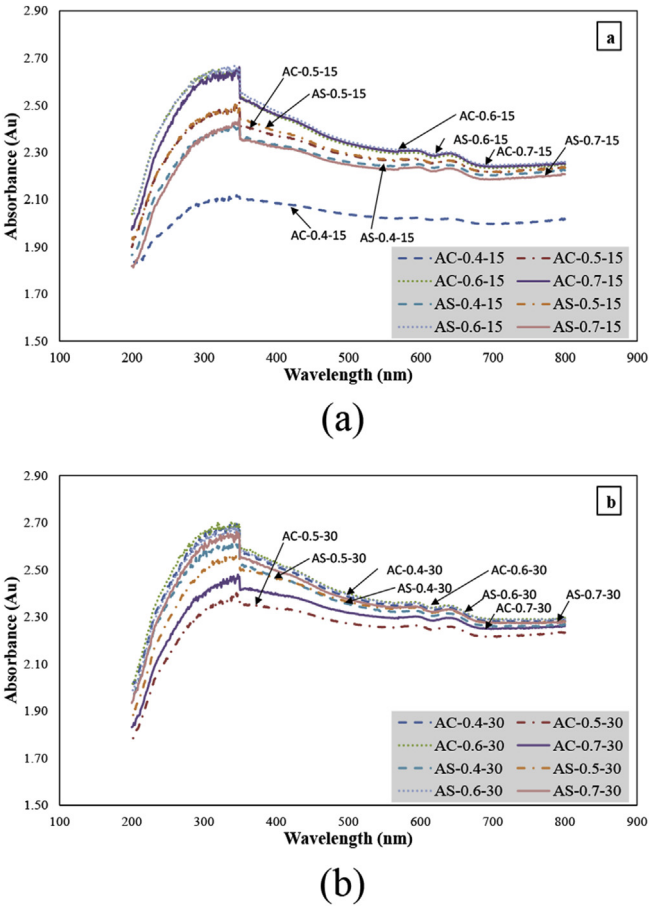

Fig. 5. Absorbance spectra of samples after sonication of (a) 15 min and (b) 30 min.

Table 2
Nomenclature used in the present study.

Nomenclature	Explanation
AC-0.4-15	S/C = 0.4, sonicated for 15 min and centrifuged for 10 min at 3000 rpm
AC-0.5-15	S/C = 0.5, sonicated for 15 min and centrifuged for 10 min at 3000 rpm
AC-0.6-15	S/C = 0.6, sonicated for 15 min and centrifuged for 10 min at 3000 rpm
AC-0.7-15	S/C = 0.7, sonicated for 15 min and centrifuged for 10 min at 3000 rpm
AS-0.4-15	S/C = 0.4, sonicated for 15 min
AS-0.5-15	S/C = 0.5, sonicated for 15 min
AS-0.6-15	S/C = 0.6, sonicated for 15 min
AS-0.7-15	S/C = 0.7, sonicated for 15 min
AC-0.4-30	S/C = 0.4, sonicated for 30 min and centrifuged for 10 min at 3000 rpm
AC-0.5-30	S/C = 0.5, sonicated for 30 min and centrifuged for 10 min at 3000 rpm
AC-0.6-30	S/C = 0.6, sonicated for 30 min and centrifuged for 10 min at 3000 rpm
AC-0.7-30	S/C = 0.7, sonicated for 30 min and centrifuged for 10 min at 3000 rpm
AS-0.4-30	S/C = 0.4, sonicated for 30 min
AS-0.5-30	S/C = 0.5, sonicated for 30 min
AS-0.6-30	S/C = 0.6, sonicated for 30 min
AS-0.7-30	S/C = 0.7, sonicated for 30 min

Table 3
Absorbance data corresponding to Fig. 5(a) and (b).

Sample name	Abs (Au)	Sample name	Abs (Au)
AC-0.4-15	2.11	AC-0.4-30	2.69
AC-0.5-15	2.51	AC-0.5-30	2.39
AC-0.6-15	2.66	AC-0.6-30	2.69
AC-0.7-15	2.44	AC-0.7-30	2.47
AS-0.4-15	2.42	AS-0.4-30	2.61
AS-0.5-15	2.49	AS-0.5-30	2.56
AS-0.6-15	2.65	AS-0.6-30	2.69
AS-0.7-15	2.66	AS-0.7-30	2.64

dispersion of CNTs in the aqueous solution. Another important aspect to be noted is that samples with S/C of 0.5 and 0.6 had similar absorbance when subjected to 15 min and 30 min agitation. These samples were well dispersed at a much faster time and remained stable after that. Hence, it can be concluded that, in order to achieve a well dispersed and stable solution, S/C ratio can be maintained between 0.5 and 0.6. Therefore, in the present study, it is considered that S/C ratio of 0.5–0.6 is the critical micelles concentration (CMC) for CNT dispersion.

In order to arrive at the optimum sonication parameters, the samples were subjected to different amplitudes and cycles. The UV–Vis absorbance spectra of solutions with different S/C ratio subjected to ultrasonication with different amplitudes and cycles is shown in Fig. 6. Initially, the sonicated and centrifuged samples were subjected to constant amplitude (50%) with varying cycles (30%–70%). It can be observed from Fig. 6(a) that in the case where cycle of 30% is imparted, the absorbance of 2.15 Au characterized by solution containing the S/C of 0.4 reduces to 1.86 Au by the solution containing S/C of 0.5. Solutions with S/C greater than 0.5 show increased absorbance. This shows that the cycle of 30% is inadequate to disperse solutions with lower S/C ratio. However, the absorbance remains almost constant for all S/C ratios when a cycle between 40% and 60% is adopted. When a cycle of 70% is employed, the absorbance increases proportionally with the change of S/C. The absorbance spectra of 40–60% cycle depict an uneven behavior whereas 70% cycle showed greater effort to untangle MWNTs through formation of uniform surfactant molecular layer covers around the nanotube surface, leads to offer better absorbance. In the further study, samples were subjected to only sonication (no centrifugation) with constant amplitude (50%) and varying cycles (30%–70%). The absorbance spectra of these samples, as shown given in Fig. 6(b), depict the huge dissimilarities due to which no meaningful conclusion could be drawn.

Similar study was carried out on AC and AS samples by varying amplitudes (30%–70%), where the cycle was kept constant at 50%. In AC sample, when the amplitude was maintained at 50%, the absorbance increases monotonically with S/C ratio. When the amplitude was at 60% and 70%, there is a monotonic increase only above the S/C ratio of 0.5. When the samples were subjected to only sonication and an amplitude of 40% was employed, a monotonic increase in absorbance with the increase in S/C ratio was noted. Further, with lesser amplitude (for example, 30%), the increase in absorbance is noticed in dispersed CNT with S/C ratio more than 0.5. However, before concluding on the influence of the parameters (such as S/C ratio, amplitude and cycle) to ultrasonication, particle size analysis was also carried out for further confirmation on observations made from the UV–Vis results.

4.2. Particle size analysis

The particle size distribution for both AS and AC samples was studied through dynamic light scattering technique (Malvern Zetasizer, nanoseries). The parameters such as viscosity and relative permittivity were chosen as reported in previous study [39,40] for carrying out the investigation on anionic surfactant (SDBS). The Z average hydrodynamic particle diameter was obtained from cumulant analysis of normalized electric field auto-correlation function.

The dynamic light scattering technique was used to measure the Z-average hydrodynamic particle diameter of both the AC and AS samples with different S/C ratios subjected to varying sonication parameters. Fig. 7(a–d) show the relation between hydrodynamic particle diameters of different S/C (0.4, 0.5, 0.6 & 0.7) dispersed MWNT suspension with respect to sonication parameter. It can be observed from Fig. 7(a–d) that in both the cases (constant amplitude, varying cycle and constant cycle, varying amplitude) when the particle is agitated at a particular range of amplitude (40–60%) and cycle (50–70%), the hydrodynamic particle size remains constant. However, this holds good only for samples with S/C ratio 0.4, 0.5 and 0.6. The sample with S/C ratio of 0.7 shows irregular behavior. This might be due to the formation of micelles owing to the higher concentration of surfactant. Due to interaction between the groups of same polarity, the micelles continue to grow larger as the concentration of surfactant increases. Identically, the same process happens on the multi-walled nanotube surface with the increase in the surfactant quantity. The MWNTs surface would have

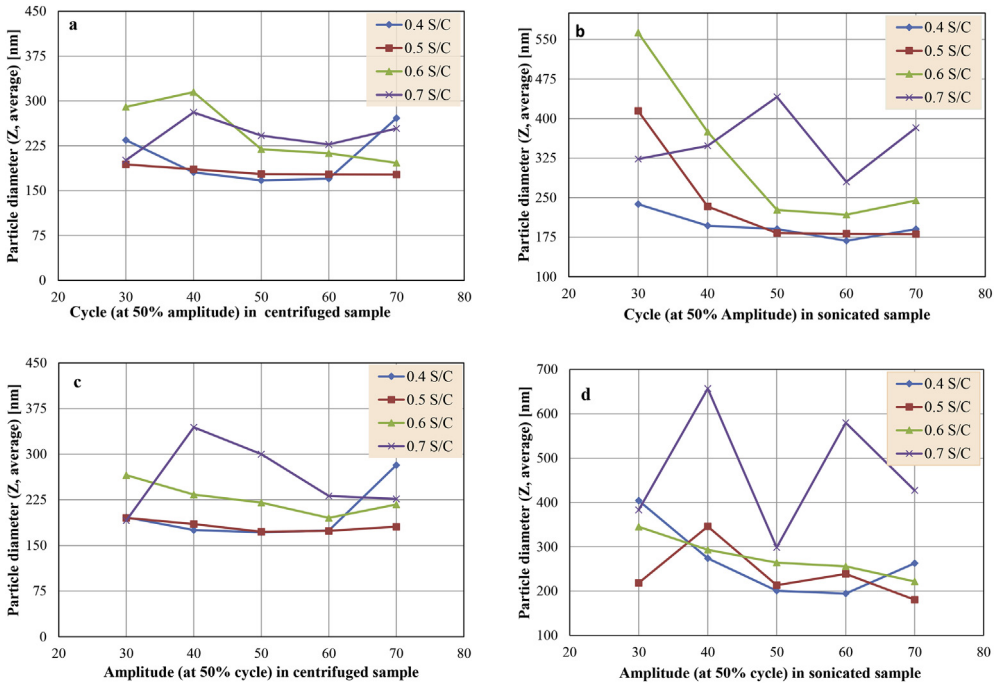

Fig. 6. The spectra of UV Vis absorbance (15 M sonication time) depends on surfactant to MWNTs ratio at varying ultrasonic cycle and amplitude. a) Centrifuged sample (const amplitude (50%), varying cycle (30, 40–70%)), b) Sonicated samples (const amplitude (50%), varying cycle (30, 40–70%)), c) centrifuged sample (varying amplitude (30, 40–70%), constant cycle (50%)), d) Sonicated samples (varying amplitude (30, 40–70%), constant cycle (50%)).

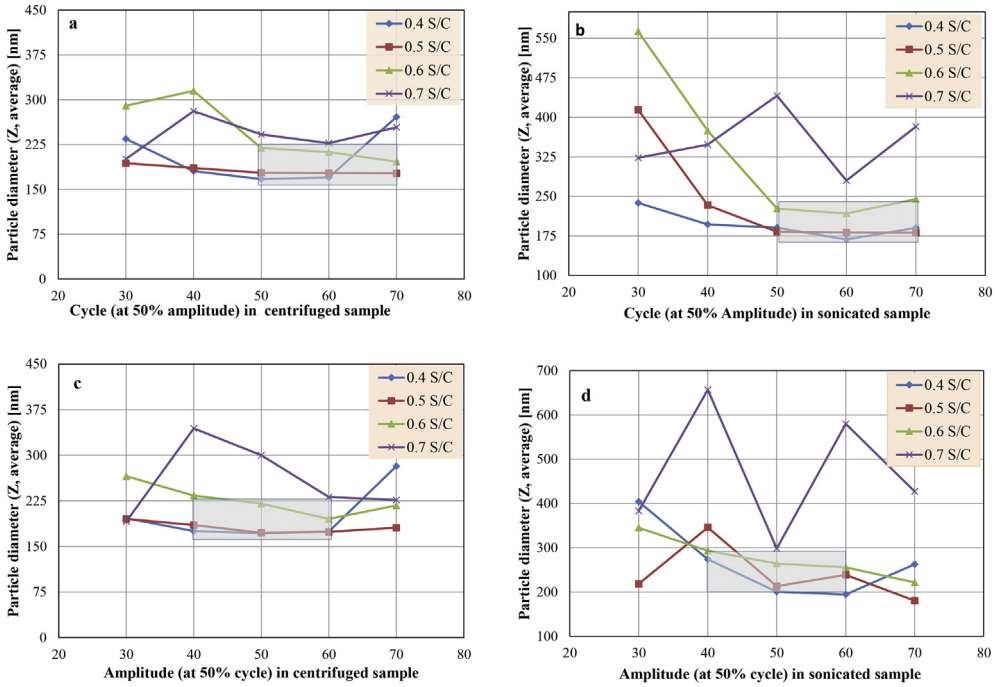

Fig. 7. The spectra of hydrodynamic diameter ($Z_{average}$) of MWNTs dispersion (15 M, 0.4, 0.5, to 0.7 S/C) depends on sonication parameters. a) Centrifuged sample (const amplitude (50%), varying cycle (30, 40–70%)), b) sonicated samples (const amplitude (50%), varying cycle (30, 40–70%)) c) centrifuged sample (varying amplitude (30, 40–70%), const cycle (50%)), d) sonicated samples (varying amplitude (30, 40–70%), const cycle (50%)).

been covered by higher amount of surfactant molecules so that the portion of surfactant molecule extended into liquid medium will start to interact with adjacent MWNTs [41,42]. This leads to decrease in the dispersion of multi-walled nanotube at high surfactant concentration. The poly-dispersive index for entire DLS analysis is listed in Table 4. The PDI value of 0.66 is obtained for AS solution with S/C ratio 0.7 when subjected to 50% amplitude and 50% cycle. This indicates that the solution contains highly non homogenous aggregates formed due to flocculation [38]. The PDI values of CNT dispersed solutions with S/C ratio of 0.5 and 0.6 are in

Table 4
Polydispersive index (PDI) estimated from the present study.

Sonication parameter (cycle or amplitude)	0.4 S/C				0.5 S/C				0.6 S/C				0.7 S/C			
	% A at Cons % C		% C at Cons % A		% A at Cons %C		% C at Cons %A		% A at Cons %C		% C at Cons % A		% A at Cons % C		% C at Cons %A	
	S	C	S	C	S	C	S	C	S	C	S	C	S	C	S	C
30	0.48	0.33	0.35	0.35	0.35	0.27	0.60	0.24	0.59	0.39	0.61	0.53	0.42	0.34	0.51	0.34
40	0.40	0.25	0.36	0.26	0.55	0.26	0.38	0.41	0.56	0.42	0.57	0.43	0.72	0.42	0.60	0.56
50	0.25	0.30	0.38	0.36	0.41	0.25	0.27	0.25	0.59	0.50	0.38	0.35	0.61	0.59	0.66	0.39
60	0.44	0.354	0.40	0.39	0.42	0.28	0.42	0.43	0.54	0.33	0.41	0.40	0.64	0.38	0.56	0.36
70	0.39	0.37	0.35	0.44	0.35	0.35	0.36	0.28	0.42	0.38	0.56	0.37	0.57	0.52	0.65	0.54

the range of 0.27–0.38. This indicates that these aggregates are comparatively more homogenous in size and better dispersed.

From the above characterisation studies, it has been identified that the following parameters may be adopted to get a reasonably good MWNT dispersed solution, (i) duration of sonication should be 30 min; (ii) S/C ratio should be between 0.5 and 0.6; (iii) amplitude of sonication should be maintained between 50% and 70%; (iv) cycle should be maintained between 40% and 50%. The observations obtained from the present study, as stated above, are used during fabrication of the test samples.

5. Test specimen fabrication

Measured quantities of cement and sand were first mixed in flat beater Hobart mixer (HL200, Humboldt Make) and mixed for few minutes to produce dry mix. Then, MWNT dispersed solution was then poured into this mixture and the remaining water (to attain the w/c ratio of 0.35) was added and mixed for 3 min. Defoamer of 0.25% of volume was then slowly added to the mixture to neutralize air voids. After the proper mix (almost 20 min of mixing in the Hobart mixer), the prepared cement mortar mix was poured into moulds of length of 160 mm, and width and height of 40 mm. The specimens were kept on a vibration table in order to achieve the required compactness. During casting, four copper electrodes (mesh size of 1.6 mm) were embedded in the specimen. Four numbers of meshes were placed inside the prism with spacing 10 mm, 40 mm and 10 mm. The specimens were de-moulded and cured under 20° C for 7 days. Before testing, the specimens were kept in oven at 60° C for 3 days to eliminate excess water content (to investigate the most adverse condition to attain the conductivity). The schematic progress of sample fabrication is shown in Fig. 8.

5.1. Electrical measurement

Four probe method was employed to measure the change in potential difference between inner copper terminals those were embedded inside the specimen. Compressive load was applied to the specimens using standard Compression Testing Machine. Test specimens were subjected to elastic-cyclic compressive loading regime with load amplitude of 5–25 kN (stress range of 2 MPa–10 MPa) at a loading rate of 40 N/s. As the specimen was subjected to cyclic compressive load, the microstructure gets altered, causing the change in potential difference between electrodes.

The electrical resistivity (ρ) of sample is measured using,

$$\rho = \frac{a}{l} \times r \tag{7}$$

where, a is area of cross section of sample (cm^2), l is the distance between inner electrodes (cm) and r is the electrical resistance (Ω). The percentage change in potential difference during cyclic compression test can be measured as,

$$\Delta V\ (\%) = \frac{V - V0}{V0} \times 100 \tag{8}$$

where, V_0 is the potential drop before loading and V is the varying potential drop at any loading time. The fractional change in electrical resistance per unit strain can be measured through two strain gauges pasted on either side of the sample. Data acquisition was carried out using computer controlled high speed MGC plus data

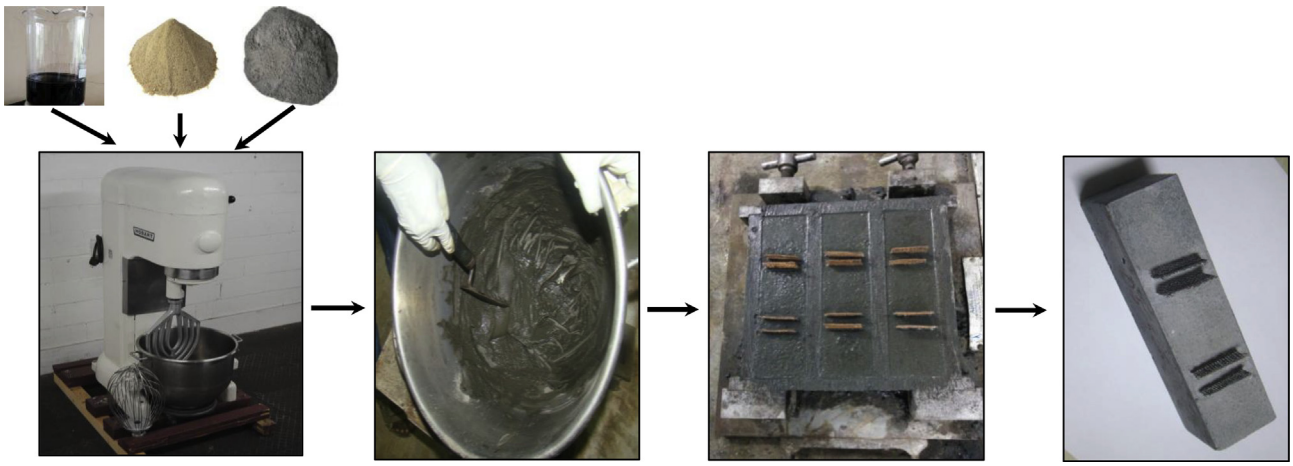

Fig. 8. Schematic process for test specimen fabrication. **(a)** Schematic sketch of experimental setup, circuit diagram with data acquisition system **(b)** Shows experimental test setup and data acquisition system.

acquisition system (using the voltage and strain channels). The circuit connection for four probe and two probe method is depicted in Fig. 9(a). The experimental setup for testing the specimen under elastic-cyclic compressive loading and data acquisition system is shown in Fig. 9(b), respectively. The rate of change of output voltage with respect to applied load for every cycle was continuously traced. The results obtained and the observations made from the study are discussed in the next section.

6. Result and discussion

The piezo-resistive response of cement nano-composite reinforced with 0.5 & 0.8 wt% of MWNTs is given in Fig. 10. Due to the lack of information in reported studies on choosing the appropriate input source, the optimum supply (DC) range is identified by investigating the conductive performance of the sample to different DC sources and monitoring its piezo-resistive response under cyclic compressive loading. The optimized DC range is obtained by tracing the steady state potential drop between the inner electrodes when subjected to different DC voltage sources (5 V, 10 V, 15 V) and current sources (1 A, 3 A and 5 A) and under cyclic compressive loading. The corresponding spectrum for input source optimization process is pictorially depicted in Fig. 10(a–f). It can be observed that when the input is 5 V and 3 A, the potential drop decreases after each cycle while maintaining its piezo-resistive characteristic. This is because of the irreversible matrix deformation under cyclic loading, caused due to the presence of micro pores in the matrix. In general, the nano-composite changes its conduction path with respect to loading direction. However, the new conducting network is formed only after deformation of the previously formed one. The continuous cyclic loading would not have allowed the matrix to fully regain to its original state before the application of load in the

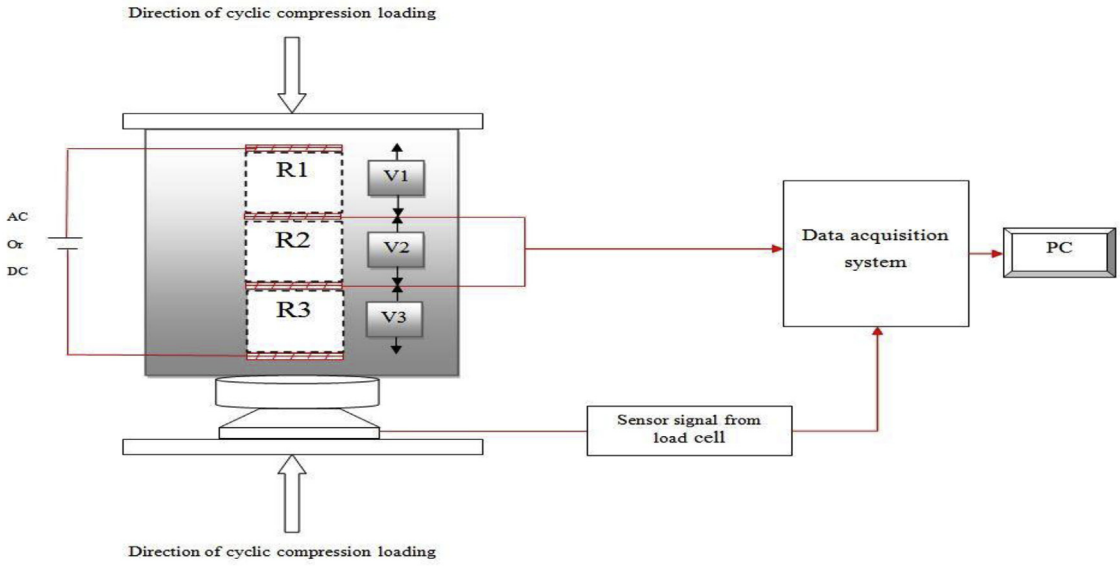

***(a)** Schematic sketch of experimental setup, circuit diagram with data acquisition system*

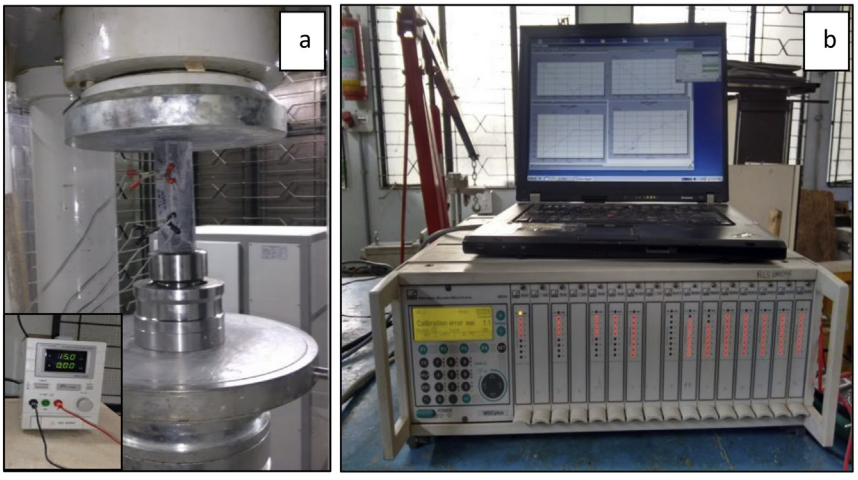

***(b)** Shows experimental test setup and data acquisition system*

Fig. 9. Experimental set up for performance evaluation of the nano composite.

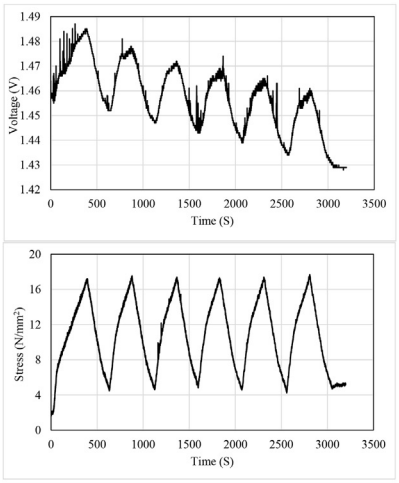

(a) piezo resistive spectra of 5V DC input

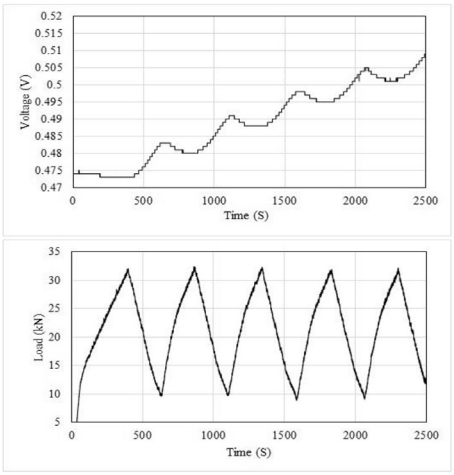

(d) piezo resistive spectra of 1A DC input

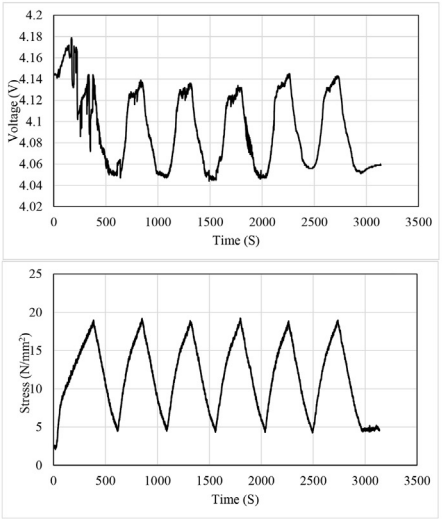

(b) piezo resistive spectra of 10V DC input

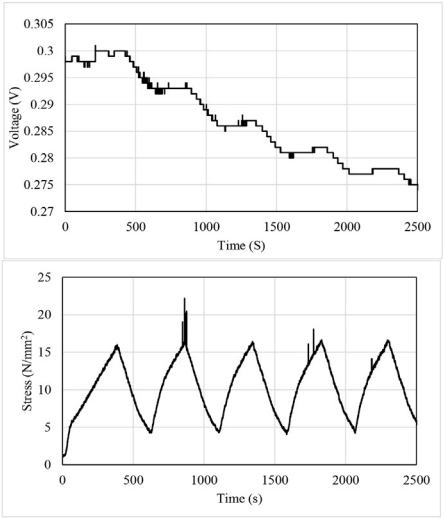

(e) piezo-resistive spectra of 3A DC input

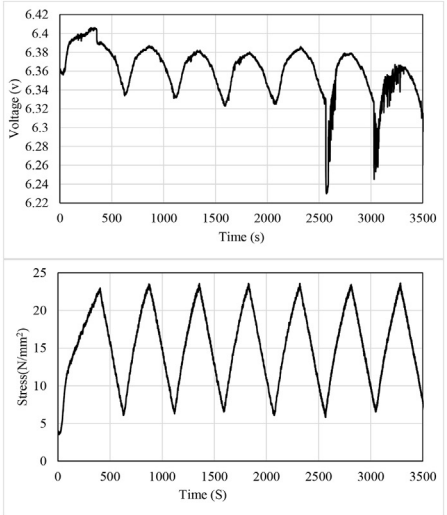

(c) piezo resistive spectra of 15 V DC input

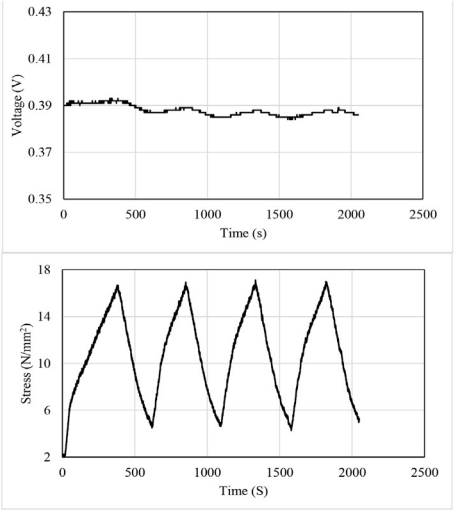

(f) piezo resistive spectra of 5A DC input

Fig. 10. Spectrum of input Source optimization for steady potential drop.

opposite direction. It is interesting to note that when the input is 1 A, the potential drop rises incrementally in successive loading cycles since the applied input is inadequate to reach the steady state rapidly, i.e., charging time constant ($\tau = RC$) is too high. When the input is 10 V, 15 V or 5 A, the nano-composite exhibits reliable steady state piezo-response characteristics by negating tunnelling conduction i.e., neutralizing barriers among CNTs successfully. However, when the input is 10 V, there is some noise at the peaks. From the above studies, it has been identified that the input of 10 V, 15 V and 5 A DC source will be optimum to achieve steady piezo-resistive characteristics in the cement based nano-composite (developed in the present study) which is nearly 75% of voltage reported earlier (Konsta Gdoutos and Aza) [43]. The guage factor of the sensor with 0.8% CNT as developed in the present study is found to be 285. It is important to mention here that, though DC source is used in the circuit of the present study, DC measurement has the drawback of polarization causing apparent increase in resistance under application of an electrical field.

Fig. 11 shows the piezo-resistive spectra of cement nano-composite reinforced with 0.5 and 0.8 wt % of CNTs. The spectrum of cement nano-composite containing 0.5 wt % of CNT shows steady piezo-resistive changes of nearly 30 mV for entire ten cycles of compressive loading. But, there is a mild drop in the potential at the end of each and every unloading regime. This is mainly due to the deformation of matrix microstructure when the specimen is under loading state. In the loading state, the particles come closer to each other leading to reduction in spacing between adjacent CNTs. This causes permanent reduction in tunnelling gap between CNTs which causes irreversible loss in potential drop in unloading state and even during the beginning of next cycle. The piezo-resistive response of 0.8 wt % MWNTs reinforced cement nano-composite is shown in Fig. 11(b). In this case, as against the earlier response obtained from 0.5 wt% MWNT, the amplitude of successive cycles increases. This might be due to the fact that increased amount of MWNTs caused creation of new conduction path under loading in negative manner (the new conduction path will be created before the deformation of already created one). Therefore, for our investigation, it has been identified that in order to create a piezo resistive cement nanocomposite, MWNTs of 0.5% weight of cement can be treated as optimum.

7. Concluding remarks

The role of ultrasonic energy and time with varying surfactant concentration on MWNTs dispersion, and piezo-resistivity of MWMTs incorporated cementitious nano-composite was studied here. It is found that the issues like process of synthesis, influence of various sonication parameters, role of ionic surfactant concentration, which are crucial to develop a composite sensor, are not adequately discussed in reported studies. In the present study, UV visible spectral description clearly depicts that longer time of sonication improves dispersion efficiency. To impart adequate ultrasonic energy and critical micelle concentration (surfactant concentration) in MWNT dispersion (for the given surfactant to MWNTs ratio of 0.5–0.6) toward uniform and stable dispersion, ultrasonic energy of 50–70% and amplitude of 50% cycle is required for centrifuged solutions, and 40% amplitude with 50% cycle is required for sonicated sample. While increasing ultrasonic energy, corresponding hydrodynamic diameter shows decreasing trend. Samples with surfactant to MWNTs ratio of 0.4–0.6 showed that the change of the sonication parameter (amplitude or cycle) did not considerably influence the hydrodynamic diameter. Due to flocculation mechanism and physical effects (temperature raise during ultrasound agitation), solutions with surfactant to MWNTs ratio of 0.7 & 0.4 (above 60% sonication parameters) showed larger hydrodynamic diameter. Also, the PDI data for sonicated sample corresponding to above discussed CMC (0.5 & 0.6) was found to be in the range of 0.2–0.3.

It is also noted that the reported studies on influence of input voltage to overcome the barrier potential of the given nano composite matrix are very scanty. However, the steady response and effective sensitivity of nano composite sensors depend on the circuit scheme with adequate input current or voltage. Experimental test results of the present study demonstrate that the piezo-resistivity of nanocomposite varies synchronously with applied load. The 15 V, 5 A input is observed as optimal ranges to achieve steady uniform piezo resistivity for both 0.5 & 0.8 wt% MWNT incorporated cement composite samples. With increase in the concentration of MWNTs (when exceeds a certain limit), the corresponding piezo-resistivity sharply changes without any additional noise. It indicates that when nanofibers exceed the percolation threshold level, these fibers facilitate direct contact

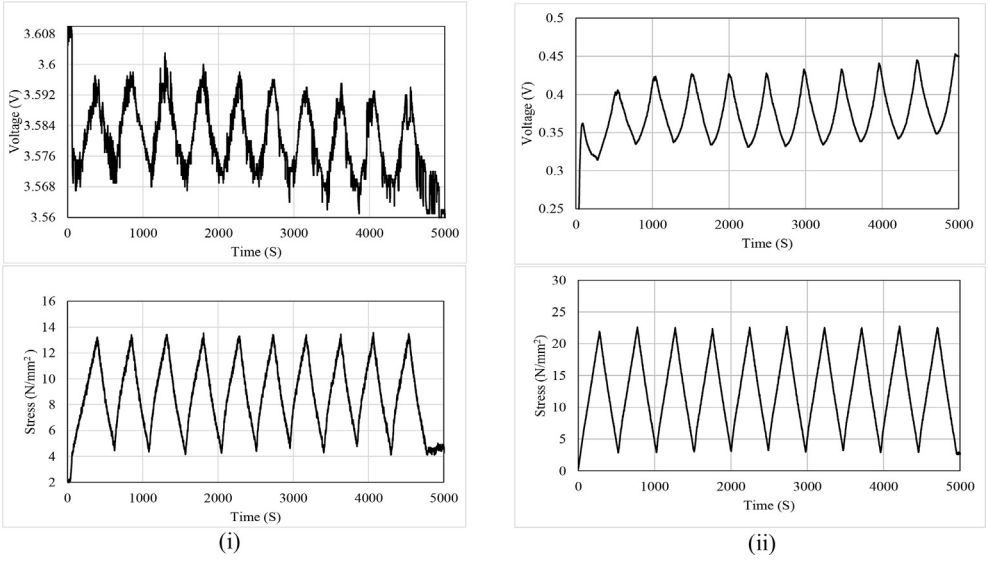

Fig. 11. Piezo resistive spectra of i) 0.5 wt% MWNTs and 0.8 wt% MWNTs incorporated samples with 15 V, 5 A DC input.

among adjacent MWNTs. The electrical conduction takes place only by direct contact of MWNTs (intrinsic properties) and the tunnelling conduction is considerably reduced. The 0.5 wt% samples showed better uniform change in piezo-resistive response without any irreversible damage than that of 0.8 wt% samples, since the 0.5 wt% MWNTs incorporated samples ensure the development of the tunnelling mechanism. Therefore, the 0.5 wt% MWNTs concentration (with appropriate sonication as described in the present study) can be adopted for developing stress sensing composite sensor. The present study provides the elaborate methodology for suitable dispersion of MWNT in the solution, preparation of cementitious nano composite and its performance as the piezo-resistive sensor. The study also indicates that much attention and inter-disciplinary contribution are further needed to develop innovative and multi-functional building materials.

References

[1] P.W. Chen, D.D.L. Chung, Carbon fiber reinforced concrete for smart structures capable of non-destructive flaw detection, Smart Mater. Struct. 2 (1993) 23–30.
[2] P.W. Chen, D.D.L. Chung, Improving the electrical conductivity of composite comprised of short conducting fiber in nonconducting matrix: the addition of nonconducting particulate filler, J. Electron. Mater. 24 (1995) 47–51.
[3] S. Hong, S. Myung, Nanotube electronics: a flexible approach to mobility, Nat. Nanotechnol. 2 (2007) 207–208.
[4] W. Obitayo, T. Liu, A review: carbon nanotube - based piezoresistive strain sensor, J. Sensors (2012) 1–15.
[5] T. Nochaiya, A. Chaipanich, Behavior of multi-walled carbon nanotubes on the porosity and microstructure of cement-based materials, Appl. Surf. Sci. 257 (2011) 1941–1945.
[6] F.H. Gojny, M.G.H. Wichmann, B. Fiedler, I.A. Kinloch, W. Bauhofer, A.H. Windle, K. Schulte, Evaluation and identification of electrical and thermal conduction mechanisms in carbon nanotube/epoxy composites, Polymer 47 (2006) 2036–2045.
[7] C.A. Coopera, R.J. Younga, M. Halsall, Investigation into the deformation of carbon nanotubes and their composites through the use of Raman spectroscopy, Compos. Part A 32 (2001) 401–411.
[8] L.A. Girifalco, M. Hodak, R.S. Lee, Carbon nanotubes, buckyballs, ropes, and a universal graphitic potential, Phys. Rev. B 62 (2000) 13104.
[9] C. Ehli, C. Oelsner, D.M. Guldi, A. Mateo-Alonso, M. Prato, C. Schmidt, C. Backes, F. Hauke, A. Hirsch, Manipulating single-wall carbon nanotubes by chemical doping and charge transfer with perylene dyes, Nat. Chem. 1 (2009) 243–249.
[10] B. Han, X. Yu, E. Know, J. Ou, Piezoresistive Multi-walled carbon nanotubes filled cement- based composites, Sens. Lett. 8 (2010) 344–348.
[11] G.Y. Li, P.M. Wang, X. Zhao, Pressure-sensitive properties and microstructure of carbon nanotube reinforced cement composites, Cem. Concr. Compos. 29 (2007) 377–382.
[12] F. Azhari, Cement-based Sensors for Structural Health Monitoring, M.S. thesis, University of British Columbia, Canada,, 2008.
[13] X. Yu, E. Kwon, Carbon-nanotube/cement composite with piezoresistive property, Smart Mater Struct. 18 (2009), 5 055010.
[14] B. Han, X. Yu, E. Kwon, A self-sensing carbon nanotube/cement composite for traffic monitoring, Nanotechnology 20 (44) (2009) 445–501.
[15] B. Han, K. Zhang, X. Yu, E. Know, J. Ou, Electrical characteristics and pressure response measurement of carboxyl MWNT/cement composites, Cem. Concr. Compos. 34 (2012) 794–800.
[16] F. Azhari, N. Banthia, Cement-based sensors with carbon fibers and carbon nanotubes for piezoresistive sensing, Cem. Concr. Compos. 34 (2012) 866–873.
[17] O. Galao, F.J. Baeza, E. Zornoza, P. Garces, Strain and damage sensing properties on multifunctional cement composites with CNF admixture, Cem. Concr. Compos. 48 (2014) 90–98.
[18] K. Parmar, M. Mahmoodi, C. Park, S.S. Park, Effect of CNT alignment on the strain sensing capability of carbon nanotube composites, Smart Mater. Struct. 22 (2013) 075006.
[19] A. Li, A.E. Bogdanovich, P.D. Bradford, Aligned carbon nanotube sheet piezoresistive strain sensors, Smart Mater. Struct. 24 (2015) 095004.
[20] F. Ubertini, S. Laflamme, H. Celan, L. Materazzi, G. Ceni, H. Saleem, A.D. Alessandro, A. Corradini, Novel nanocomposite technologies for dynamic monitoring of structure: a comparison between cement based embeddable and soft elastomeric surface sensors, Smart Mater. Struct. 23 (2014) 045023.
[21] L. Brown, Florence Sanchez, Influence of carbon nanofiber clustering on the chemo-mechanical behaviour of cement pastes, Cem. Concr. Compos. 65 (2016) 101–109.
[22] R.N. Howser, H.B. Dhonde, Y.L. Mo, Self-sensing of carbon nanofiber concrete columns Subjected to reversed cyclic loading, Smart Mater. Struct. 20 (2011) 085031.
[23] R. Nadiv, M. Shtein, M. Refaeli, A. Peled, O. Regev, The critical role of nanotube shape in cement composites, Cem. Concr. Compos. 71 (2016) 166–174.
[24] A.L. Materazzi, F. Ubertini, A. D'Alessandro, Carbon nanotube cement-based transducers for dynamic sensing of strain, Cem. Concr. Compos. 37 (2013) 2–11.
[25] F. D'Alessandro, A.L. Ubertini, S. Materazzi, Laflamme M. Porfiri, Electromechanical modelling of a new class of nanocomposite cement-based sensors for structural health monitoring, Struct. Health Monit. 24 (2014), 1475921714560071.
[26] J. Luo, Z. Duan, H. Li, The influence of surfactants on the processing of multi-walled carbon nanotubes in reinforced cement matrix composites, Phys. Status Solidi A 206 12 (2009) 2783–2790.
[27] B. Krause, M. Mende, P.P. Tschke, G. Petzold, Dispersability and particle size distribution of CNTs in an aqueous surfactant dispersion as a function of ultrasonic treatment time, Carbon 48 (2010) 2746–2754.
[28] B. Han, X. Yu, Effect of surfactant on pressure-sensitivity of CNT filled cement mortar composites, Front. Mater. 27 (1) (2014) 1–5.
[29] B. Zou, S.J. Chen, A.H. Korayem, F. Collins, C.M. Wang, W.H. Duan, 2015 Effect of ultrasonication energy on engineering properties of carbon nanotube reinforced cement pastes, Carbon 85 (2015) 212–220.
[30] B. Han, K. Zhang, T. Burnham, E. Kwon, X. Yu, Integration and road tests of a self-sensing CNT concrete pavement system for traffic detection, Smart Mater. Struct. 22 (2013) 015020.
[31] A.D. Alessandro, M. Rallini, F. Ubertini, L.A. Materazzi, J.M. Kenny, Investigations on scalable fabrication procedures for self-sensing carbon nanotube cement-matrix composites for SHM applications, Cem. Concr. Compos. 65 (2016) 200–213.
[32] C. Feng, L. Jiang, Micromechanics modelling of electrical conductivity of carbon nanotube (CNT) – polymer nanocomposite, Compos. Part A Appl. Sci. Manuf. 47 (2013) 143–149.
[33] K.Y. Yan, Q.Z. Xue, Q.B. Zheng, L.Z. Hao, The interface effect of the effective electrical conductivity of carbon nanotube composites, Nanotechnology 18 (2007) 255705.
[34] D.J. Yang, S.G. Wang, Q. Zhang, P.J. Sellin, G. Chen, Thermal and electrical transport in multi-walled carbon nanotubes, Phys. Lett. A 329 (2004) 207–213.
[35] C. Li, E.T. Thostenson, T.W. Chou, Dominant role of tunneling resistance in the electrical conductivity of carbon nanotube–based composites, Appl. Phys. Lett. 91 (2007) 223114.
[36] M.F. Islam, E. Rojas, D.M. Bergey, A.T. Johnson, A.G. Yodh, High weight fraction surfactant solubilization of single–wall carbon nanotubes in water, Nano Lett. 3 (2003) 269.
[37] J.F. Liu, W.A. Ducker, Self-assembled supramolecular structures of charged polymers at the graphite/liquid interface, Langmuir 16 (7) (2000) 3467–3473.
[38] R. Rastogi, R. Kaushal, S.K. Tripathi, A.L. Sharma, I. Kaur, L.M. Bharadwaj, Comparative study of carbon nanotube dispersion using surfactants, J. Colloid. Interface Sci. 328 (2008) 421–428.
[39] Y. Iwadare, T. Suawa, ζ – potentials of Natural and synthetic fiber in SDS solution and the viscosity of SDS solution above the critical Micelle concentration, Bull. Chem. Soci. Jpn. 43 (1970) 2326–2331.
[40] M. Perez-Rodrıguez, L.M. Varela, M. Garcıa, V. Mosquera, F. Sarmiento, Conductivity and relative permittivity of sodium n-dodecyl sulfate and n-dodecyl trimethylammonium bromide, J. Chem. Eng. Data 44 (1999) 944–947.
[41] M.J. Rosen, Surfactants and Interfacial Phenomena, Wiley–Inter science, New York, 1987.
[42] P. Somasundaran, T.W. Healy, D.W. Fuerstenau, The aggregation of colloidal alumina dispersions by adsorbed surfactant ions, J. Colloid Interface Sci. 22 (1966) 599.
[43] M.S. Konsta – Gdoutos, C.A. Aza, Self sensing carbon nanotube (CNT) and nanofiber (CNF) cementitious composites for real time damage assessment in smart structures, Cem. Concr. Compos. 53 (2014) 162–169.